An Algorithm for Correcting Systematic Energy Deficits in the Atom Probe Mass Spectra of Insulating Samples*

Benjamin W. Caplins[a,*], Paul T. Blanchard[b], Ann N. Chiaramonti[a], David R. Diercks[b,c], Luis Miaja-Avila[b], Norman A. Sanford[b]

[a] *National Institute of Standards and Technology, Applied Chemicals and Materials Division, Boulder, CO, 80305, United States*
[b] *National Institute of Standards and Technology, Applied Physics Division, Boulder, CO, 80305, United States*
[c] *Colorado School of Mines, Metallurgical and Materials Engineering, Golden, CO, 80401, United States*

Abstract

Improvements in the mass resolution of a mass spectrometer directly correlate to improvements in peak identification and quantification. Here, we describe a post-processing technique developed to increase the quality of mass spectra of strongly insulating samples in laser-pulsed atom probe microscopy. The technique leverages the self-similarity of atom probe mass spectra collected at different times during an experimental run to correct for electrostatic artifacts that present as systematic energy deficits. We demonstrate the method on fused silica (SiO_2) and neodymium-doped ceria (CeO_2) samples which highlight the improvements that can be made to the mass spectrum of strongly insulating samples.

Keywords: atom probe microscopy; field ion microscopy; insulators; computational methods

1. Introduction

The laser-pulsed atom probe microscope is one of the most powerful tools in materials science. In concept, it can deconstruct a nanoscale sample one atom at a time; then, computational methods can be used to reconstruct the probed volume with the atomic coordinates and isotopic mass of each atom. This atomic scale reconstruction can give detailed insight into how material composition varies at the nanoscale. In practice, however, many technical challenges need to be solved to get an accurate three-dimensional atomic reconstruction, including correcting for various geometric artifacts and accurate ranging/quantification of the associated mass spectra. In this manuscript, we present a computational post-processing algorithm to improve the quality of mass spectrometry data derived from electrically insulating specimens which can be prone to electrostatic artifacts.

In the laser-pulsed atom probe microscope, an atomically sharp tip is placed near a local electrode (Figure 1). The local electrode is electrically biased with a DC voltage (V_{app}) such that the surface atoms on the tip are held just below the threshold required for field evaporation. A short laser pulse provides the necessary stimulus to trigger field ion emission, and the resulting ion is accelerated to the detector which measures the ion's time-of-flight. The flight time is related to the flight path length, the ion's mass-to-charge ratio, and the bias voltage between the tip and the electrode. For conical tips, the radius of curvature of the tip will change as the tip is eroded and the bias voltage is typically adjusted to keep some observable (such as detection rate or charge-state ratio which are related to the surface field) constant. As a result of the bias voltage varying throughout an experiment, ions that have the same mass-to-charge ratio (m/z, dalton/electron charge) will have varying flight times. Thus, the exact acceleration voltage of each ion must be considered in order

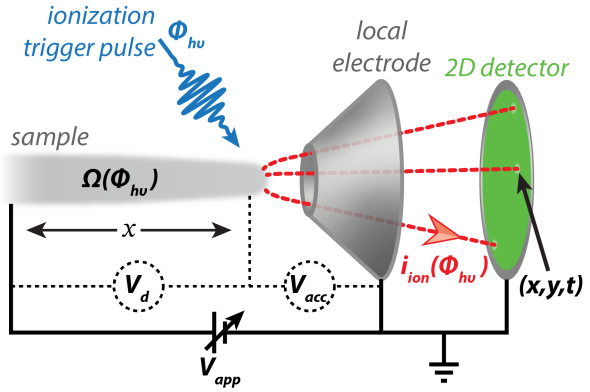

Figure 1: Schematic of the experiment. A DC voltage (V_{app}) is applied to a nanoscale tip relative to a local electrode. A laser pulse triggers field ion evaporation. The ion is accelerated to the detector by a voltage (V_{acc}) that is slightly less than the applied voltage. A voltage drop (V_d) exists over the tip due to the ion current and resistivity of the tip. The acceleration voltage is thus a function of the ion current and the resistivity of the sample – both of which are potentially a function of the laser irradiance.

*Contribution of NIST, an agency of the US government; not subject to copyright in the United States.

*Corresponding Author
Email address: benjamin.caplins@nist.gov (Benjamin W. Caplins)

dataset	1	2	3	4
material	steel	SiO_2	SiO_2	Nd-doped CeO_2
pulse frequency	250 kHz	500 kHz	250 kHz	625 kHz
temperature	29 K	57 K	57 K	46 K
pulse energy	20 pJ	150 pJ	10 pJ - 250 pJ	100 fJ
pressure	4.8×10^{-9} Pa	3.3×10^{-9} Pa	1.6×10^{-8} Pa	8.8×10^{-9} Pa
detection rate	0.5 %	0.2 %	0.02 % - 0.2 %	0.3 %
laser tracking	enabled	enabled	disabled	enabled
voltage feedback	enabled	enabled	disabled	enabled
figures	2a	2b, 4, 5, 6a-c, 7	3	6d-f, 7

Table 1: Experimental parameters for atom probe datasets.

to convert the time-of-flight data to mass-to-charge ratio data.[1, 2, 3, 4] In addition, the variation in flight lengths that occur due to the geometric projection of a point emitter onto a planar detector must be accounted for in the calculation of the m/z for each ion.[1, 2, 3, 4]

In principle, the exact voltage and flight length for each ion event are accounted for as the time-of-flight is converted to mass-to-charge ratio:[1, 2, 3, 4]

$$\frac{m}{z} = \frac{2\,e\,V_{\text{app}}}{L^2} t_{\text{obs}}^2 \tag{1}$$

where V_{app} is the applied voltage, L is the ion flight length, e is the charge of an electron, and t_{obs} is the observed ion flight time.[1] In practice, however, the flight times are typically 'voltage' and 'bowl' corrected – which means that the effect of the voltage (V_{app}) and geometry (L) on the flight times are removed. In this case, the observed time-of-flight data is transformed into a fictitious 'corrected' time-of-flight space prior to computing the m/z values. All atom probe analysis software must apply the voltage and bowl corrections to attain high mass resolving power. In this manuscript, all data have been bowl corrected to highlight the remaining corrections that still need to be made prior to analysis.

In an atom probe experiment, the m/z of the ions are calculated according to Eq 1 which can be rewritten as:

$$\frac{m}{z} = \frac{2\,e\,V_{\text{ref}}}{L^2} \left(t_{\text{obs}} \times \sqrt{\frac{V_{\text{app}}}{V_{\text{ref}}}} \right)^2 = \frac{2\,e\,V_{\text{ref}}}{L^2} t_{\text{corr}}^2 \tag{2}$$

where V_{ref} is a (somewhat arbitrary) reference voltage and t_{corr} is a 'corrected' flight time. Thus, to the first order, the voltage correction is quite simple. Each ion's flight time can just be scaled by a value proportional to the square root of the acceleration voltage:

$$t_{\text{corr}} = t_{\text{obs}} \times \sqrt{\frac{V_{\text{app}}}{V_{\text{ref}}}} \tag{3}$$

[1]Note that in this manuscript the conversion from SI units (kg/C) to the conventional mass-to-charge ratio (m/z) is implied in the equations for notational simplicity.

In practice, a slightly more complex correction is frequently used as it captures the experimental variations more accurately:[2, 3]

$$t_{\text{corr}} = t_{\text{obs}} \times a_0 \sqrt{a_1 + V_{\text{app}} + a_2 V_{\text{app}}^2} \tag{4}$$

The parameters, $\{a_n\}$, have the units necessary for the correct dimensional analysis and are chosen to minimize the peak widths in the 'corrected' time-of-flight spectrum. In practice, this correction works well for conductive samples, but we have found that it sometimes works poorly for insulating samples.

In order to understand why the voltage correction is straightforward for the conductive samples, but not for the insulating samples, we consider basic arguments (Figure 1). The field evaporation of ions creates an ion current from the tip apex to the detector, and the light pulse can generate photocarriers. Thus, there is a voltage drop (V_{d}) along the tip that is explicitly a function of ion current (i_{ion}) and resistivity (Φ) and implicitly a function of the laser irradiance ($\Omega_{h\nu}$). The voltage drop means that an ion is actually accelerated with a potential less than that of the applied voltage:

$$V_{\text{acc}} = V_{\text{app}} - V_{\text{d}}\left(i_{\text{ion}}(\Phi_{h\nu}), \Omega(\Phi_{h\nu})\right) \tag{5}$$

For materials with low electrical resistance, e.g. metals, the voltage drop along the tip associated with this ion current will generally follow Ohm's law and is negligible. However, for materials with extremely high resistance, e.g. SiO_2, the attoamp to femtoamp ion currents can lead to significant voltage drops which may not necessarily even follow Ohm's law.[5] A time-invariant voltage drop can be accommodated by the a_1 fit parameter in Eq 4, but fluctuations in the ion current or resistivity that occur during an experiment cannot be accounted for. During a laser-pulsed atom probe experiment, these fluctuations are caused, at least in part, by laser-induced photoconductivity, as noted previously and demonstrated below.[6, 7, 8, 5] Herein, we demonstrate example cases where the voltage correction outlined above is insufficient, broadly discuss the reasons why this is occurs, and present a new correction algorithm.

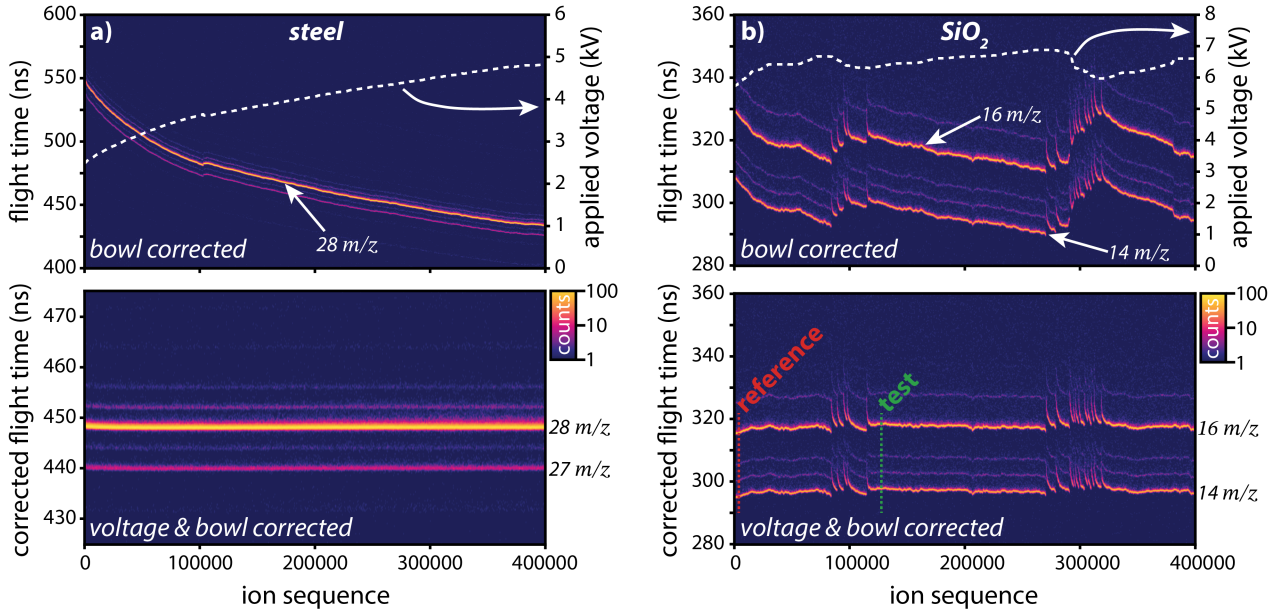

Figure 2: (a) The time-of-flight history for a steel sample with and without the voltage correction. The applied voltage is overlaid as a dashed line. Once the voltage correction (Eq. 4) is applied, the peak flight times are constant throughout the experiment. The peaks at 27 m/z and 28 m/z are $^{54}Fe^{2+}$ and $^{56}Fe^{2+}$ respectively. (b) The time-of-flight history for an SiO_2 sample with and without the voltage correction. The applied voltage is overlaid as a dashed line. Unlike the steel dataset, the voltage correction is insufficient to ensure the peak flight times are constant throughout the experiment. The peaks at 14 m/z and 16 m/z are $^{28}Si^{2+}$ and $^{16}O^{+}$ respectively. The two dotted lines labeled 'reference' and 'test' are referenced when a computational method is described, *vide infra*. Note, all time-of-flight histories in this manuscript have been bowl corrected and are displayed on a logarithmic color scale.

2. Experimental

Two atom probe microscopes were used in the this study – both were 90 mm straight flight path local electrode atom probes (LEAP 4000X-Si, CAMECA) equipped with a 355 nm pulsed laser.[2] Four different datasets were collected for this manuscript. The experimental parameters for these are given in Table 1. Using commercial software (IVAS 3.8.4, CAMECA) the data were exported to the 'epos' file format[1, 2, 3] for custom processing. The proposed computational method is implemented in Python 3.7 and code is provided in the supplementary material.

3. Laser Dependent Voltage Drop in SiO_2 Tips

Figure 2a shows the time-of-flight data for a steel sample with and without the voltage correction. The dashed line shows the voltage evolution, and the 2D intensity plot shows the time-of-flight history of the 28 m/z ($^{56}Fe^{2+}$) peak. The voltage evolution and the ion time-of-flight are (inversely) correlated and once the voltage correction is applied, the peak flight time appears constant for the entire dataset. In contrast, Figure 2b shows the voltage evolution and time-of-flight history for the 14 m/z ($^{28}Si^{2+}$) and 16 m/z ($^{16}O^{+}$) peaks from a SiO_2 sample with and without the voltage correction. While the voltage correction removed some of the low frequency flight time fluctuations, it was unable to remove all the fluctuations.

The SiO_2 data in Figure 3 show the time-of-flight history for the 16 m/z ($^{16}O^{+}$) peak. The V_{app} was held constant, except for a small change in the middle of the run. In the first half of the run, the pulse energy was briefly lowered from 250 pJ to 25 pJ and 10 pJ, as noted. When the pulse energy was lowered, the flight times increased and the detection rate decreased. This behavior is in agreement with previous work which found a photoconductive effect for SiO_2 and MgO.[7, 8] Thus, when the laser pulse energy is decreased (and the voltage is held constant), the electrical conductivity decreases, and the voltage drop increases – causing a smaller acceleration voltage and longer flight times. The same general phenomenon occurs when the laser spot is shifted off of the tip, as shown in the second half of the dataset, and is again consistent with a photoconductive-like effect.[7, 8, 5] We note that most atom probe instruments have computer control loops that endeavor to keep the laser focus on the sample tip. In order to accomplish this, the control loop routinely rasters the beam in space and modifies the beam focus. These computer controlled scans appear to cause the discontinuous jumps in Figure 2b.

It is likely that Ohm's law and the photoconductive effect are insufficient to fully understand the potentially non-equilibrium behavior that may occur at nanoscale in-

[2]Commercial instruments, equipment, or materials are identified only in order to adequately specify certain procedures. In no case does such an identification imply recommendation or endorsement by NIST, nor does it imply that the products identified are the best available for the purpose.

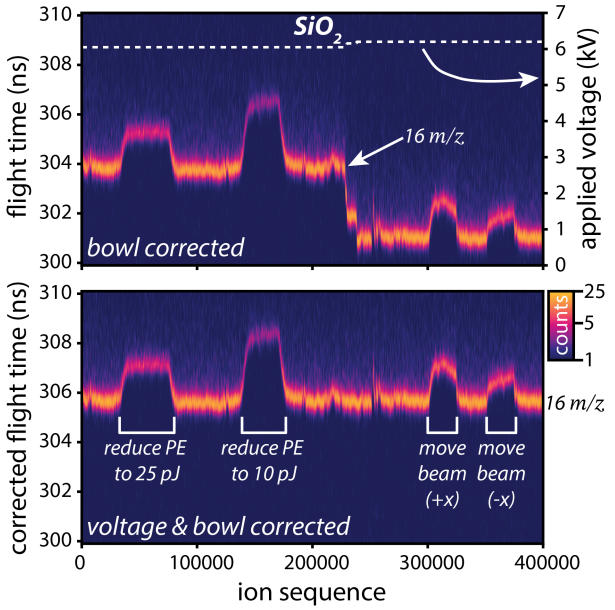

Figure 3: The time-of-flight history for an SiO_2 sample with and without the voltage correction. The applied voltage is overlaid as a dashed line. The voltage was mostly constant, and the voltage correction is insufficient to ensure the peak flight times are constant throughout the experiment. The nominal pulse energy (PE) was 250 pJ and the nominal beam location was on the tip. The pulse energy was briefly reduced to 25 pJ and 10 pJ as noted and the peak flight times increased. The beam was briefly walked off of the tip (along the tip axis) in the positive and negative x-direction as noted and the peak flight times increased. This demonstrates the laser is capable of changing the peak flight times independent of the voltage.

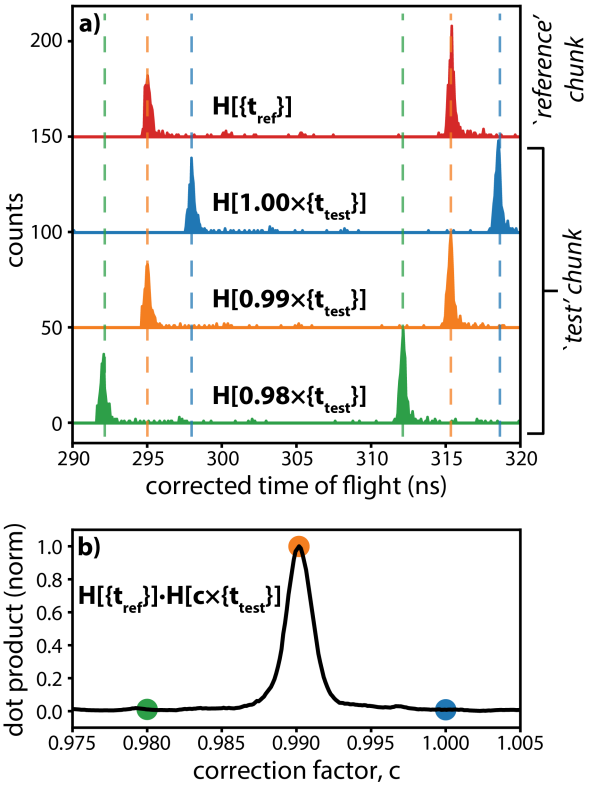

Figure 4: (a) Histograms (denoted as H[·]) of the two 'chunks'. The 'reference' chunk histogram is computed without any correction factor. The 'test' chunk histograms were computed using three different correction factors (1.00 (i.e. no correction), 0.99, and 0.98) to visualize their effect. A correction factor of 0.99 visually aligns the reference and test data. (b) The dot product between the reference and test histograms was computed for a range of correction factors. The optimal correction factor occurs when the dot product (i.e. overlap integral) is maximized.

sulating tips with attoamp to femtoamp ion currents.[5] However, they support the notion that the intensity distribution of the laser at the sample can affect ion flight times through a voltage-drop effect. The data clearly demonstrate that the laser plays an important role in determining this voltage drop. Notably, this effect can *never* be accounted for with any function that depends solely on the applied voltage bias (e.g. the voltage correction given in Eq 4). The voltage-drop effect observed here can be considered a type of systematic 'energy deficit' (i.e. an inconsistency between the applied voltage and the ion's kinetic energy) and would not be expected to occur when using an energy compensating detector.[9, 10]

4. A Systematic Energy Deficit (SED) Correction Algorithm

Three options exist to remove perturbations to the ion flight times in atom probe data. First, a theoretical or phenomenological model could be developed that incorporates the exact laser intensity distribution and the material properties. Practically, this is difficult because the material properties of nanoscale insulating tips under high applied fields and non-equilibrium conditions are unknown and the laser intensity distribution on the sample is not directly measured. Second, the effect could potentially be removed experimentally. For example by coating the tip with a thin conducting layer.[11, 8] Alternatively, reflectron based detectors remove/reduce the dependence of the measured time-of-flight on the ion's kinetic energy.[10, 1, 2, 3] These experimental solutions add cost/complexity, however, and cannot be performed after the data have been collected.

Finally, the data can be corrected empirically – i.e. a multiplicative correction factor can be applied to each ion's flight time in order to remove the influence of the (unknown) varying acceleration voltage. While scientifically this is the most unsatisfying of the three options, it is by far the most practical. Thus, we develop below a method to correct the time-of-flight data for the varying acceleration voltage that may occur when examining insulating samples. To differentiate it from the 'bowl' and 'voltage' corrections, we refer to this as the 'systematic energy deficit' (SED) correction. A Python implementation of the algorithm is available online.[12]

The physical basis for correcting the time-of-flight data for a fluctuating acceleration voltage relies on the basic fact that the isotopic mass is constant for a given ele-

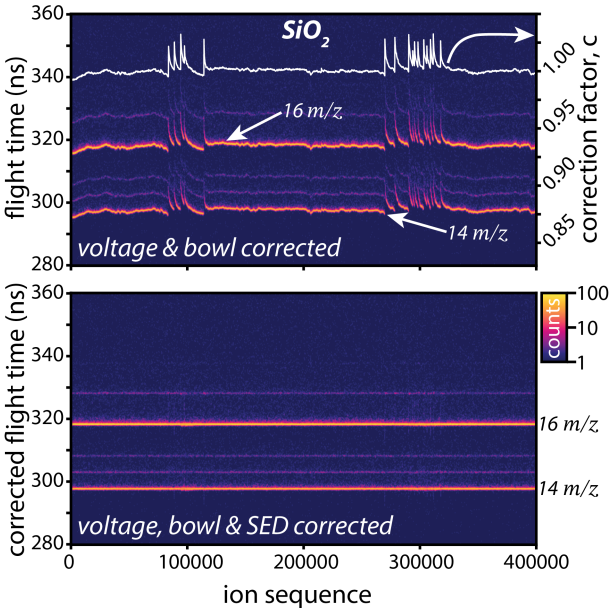

Figure 5: The time-of-flight history (same data as Figure 2b) for an SiO_2 sample with (bottom) and without (top) the systematic energy deficit (SED) correction. The correction factors are overlaid as a solid line. Once the SED correction is applied, the peak flight times are constant throughout the experiment as would be expected.

ment. Hence, if the mass spectrum is altered in a recognizable manner as a function of time, then (assuming the path length is fixed) it can be surmised that the acceleration voltage has changed. The problem then becomes developing an algorithm to find the multiplicative correction factors (i.e. the relative change in V_{acc}) that track the motion of the spectrum over the course of an experiment. Notably, the method described below assumes that there exists a voltage drop but does not assume any particular physical model for it (e.g. Ohmic versis Poole-Frenkel[13, 5]).

We first present how the method works in concept, before describing how it is performed computationally.

The first step is to segment the time-of-flight data into contiguous 'chunks'. For example, in Figure 2b we identify two distinct chunks each containing $N = 1024$ ions. The time-of-flight histograms for the first 'reference' chunk is shown at the top of Figure 4a. The time-of-flight data for the 'test' chunk is accumulated into a histogram and plotted immediately below the reference chunk histogram. The test chunk is not aligned to the reference chunk – the flight times are systematically longer. In the lower half of 4a, the test chunk data is scaled by a multiplicative correction factor prior to being accumulated into a histogram and plotted. A correction factor of 0.99 appears to align the peaks in the test chunk histogram to the peaks of the reference chunk histogram, whereas a correction factor of 0.98 or 1.00 (i.e. no correction factor) results in misaligned histograms. The dot product between the reference and test histograms is computed and used as a figure of merit that can be maximized to find the best alignment. The dot product is chosen here because the Cauchy-Schwartz inequality,

$$|\langle \mathbf{u}, \mathbf{v} \rangle| \leq \|\mathbf{u}\| \, \|\mathbf{v}\| \tag{6}$$

guarantees that the dot product is maximized only when the histograms (i.e. the vectors $\mathbf{u}$ and $\mathbf{v}$) are linearly dependent. The dot product is plotted as a function of the correction factor (Figure 4b) and it shows a sharp maximum near 0.99. Therefore, in order to align these two chunks of data, the time-of-flight data in the test chunk should be scaled by 0.99. To put this in context, for a peak at 100 m/z, a 0.99 time-scaling correlates to a shift of 2 m/z.

The procedure to extend this idea to correct a full dataset (instead of a single chunk) follows. First the histogram for a full dataset is computed – this histogram will serve as the 'reference' histogram. Then the full dataset is divided into chunks where each chunk contains N events. Next, the correction factor that aligns each individual 'test' chunk to the reference histogram is determined using the procedure outlined above (Figure 4). Once the correction factors for each chunk are known they can be interpolated and applied to each individual event to create a fully corrected dataset. This process can then be iterated if necessary, using the new corrected dataset to create a new reference spectrum; in practice, for the SiO_2 and CeO_2 data we have examined we have found 2 iterations to be sufficient.

In practice, the process of multiplying time-of-flight data by a correction factor, creating a histogram, and taking a dot product is computationally expensive and is probably not viable for large datasets. Instead, the (voltage, bowl, and t_0-corrected) time-of-flight data is log transformed – thus, a multiplicative constant becomes an additive constant. This log-transform enables us to then leverage standard fast Fourier transform (FFT) based cross-correlation algorithms to do an exhaustive search to find the optimal shift (correction factor).[14] Using the FFT significantly improves the speed and robustness of the optimization versus using a nonlinear optimization.

Using the Fourier based method, datasets with 1 million ions can be corrected in ca. 10 s on a desktop computer (6 cores, 3.5 GHz) and the computational complexity scales linearly with the dataset size.

The results of applying this algorithm (with $N = 128$) to the data in Figure 2b are shown in Figure 5 (top). The bowl- and voltage-corrected data is shown overlaid with the computed correction factor. Visually, the correction factor tracks the changing flight times quite well. If these correction factors are interpolated to correct each event in the full dataset then the result is shown in Figure 5 (bottom). The peak flight times in the fully corrected dataset do not appear to change over the duration of the experiment demonstrating that the correction has succeeded.

The mass spectra of the corrected and uncorrected SiO_2 data are shown in Figure 6a-c. The uncorrected data display significantly broader peaks with an extra (unphysical)

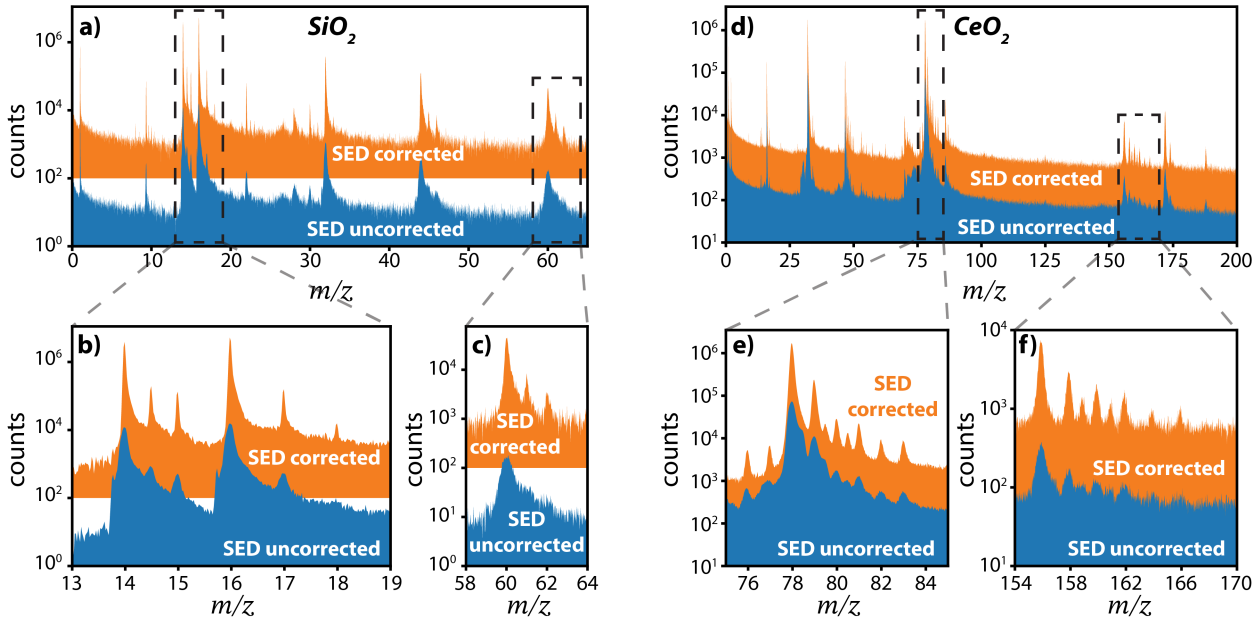

Figure 6: (a-c) Mass spectra for the SiO_2 dataset (same data as Figure 2b) corrected and uncorrected for the voltage-drop effect. The SED correction removed the spurious peaks that show up on the low m/z side of each major peak and significantly reduces the peak widths. The peaks at 61 m/z and 62 m/z become narrow enough that they emerge from the noise floor. (d-f) Mass spectra for a CeO_2 dataset corrected and uncorrected for the voltage-drop effect. The many isotopic peaks are merged together in the uncorrected spectrum, but are easily distinguished in the corrected spectrum.

peak appearing on the low m/z side of the major peaks. The peak at 18 m/z that is apparent in the corrected data is absent in the uncorrected data. The isotopic peaks at 61 m/z and 62 m/z are unresolved in the uncorrected data, while they are easily resolved in the corrected data. A second dataset on a CeO_2 sample (Figure 6d-f) shows a similar trend, with the complex isotopic distributions being easily resolved in the corrected data and difficult to resolve in the uncorrected data.

5. Selecting the Chunk Size

In practice, a potential difficulty of using this correction algorithm is in selecting an appropriate chunk size parameter N (the number of ions per chunk). For values of N that are too large, the correction will be ineffective at removing voltage-drop artifacts; the extreme case being a chunk size that is equal to the dataset size, meaning that no correction is performed. Alternatively, for values of N that are too small, the model will overfit the data – i.e. the number of parameters in the model will be too high to support the information content of the data. This could, for example, result in the peaks being unphysically narrow, with the extreme case being $N = 1$ where the data would be corrected into a single delta function. Pragmatically, we found that $N = 1024$ seemed to give visually reasonable corrections for all the data we studied, but removing user bias from this parameter selection would, of course, be ideal.

To objectively determine an appropriate chunk size for a given dataset, we apply a machine learning technique known as validation.[15] We start by splitting our dataset up into a training dataset and a validation dataset; here we split the data up by placing odd indexed events in the training set and even indexed events in the validation set. Then, the training set is used to find the correction factors for a range of chunk sizes. We then apply these correction factors to the validation dataset and compute a metric for how well the data is concentrated into peaks. Here, we use the χ^2 statistic to compare the histogram to a uniform distribution – higher values of the χ^2 statistic indicate the histogram is less 'uniform' in nature, and thus more 'peaked'. Thus, a maximum in a plot of the χ^2 statistic versus chunk size yields an estimate of the 'best' chunk size which is free from user selection. The plot of χ^2 statistic versus N for the CeO_2 and SiO_2 datasets is shown in Figure 7 (top). For comparison, the normalized mass-resolving power (MRP) (computed at full width at half maximum) for the two most prominent peaks in each dataset are show in Figure 7 (bottom). The maximum for the MRP corresponds to that of the χ^2 statistic. In practice we prefer the χ^2 statistic for the determination of the optimal N because it measures the 'peaked-ness' of the full mass spectrum as opposed to the single width measurement of single peak and is therefore more robust. In our analysis, we use a chunk size double that of the one that corresponds to a maximal value of χ^2 in order to account for any potential bias due to the fact that the dataset was divided in half for training/validation.

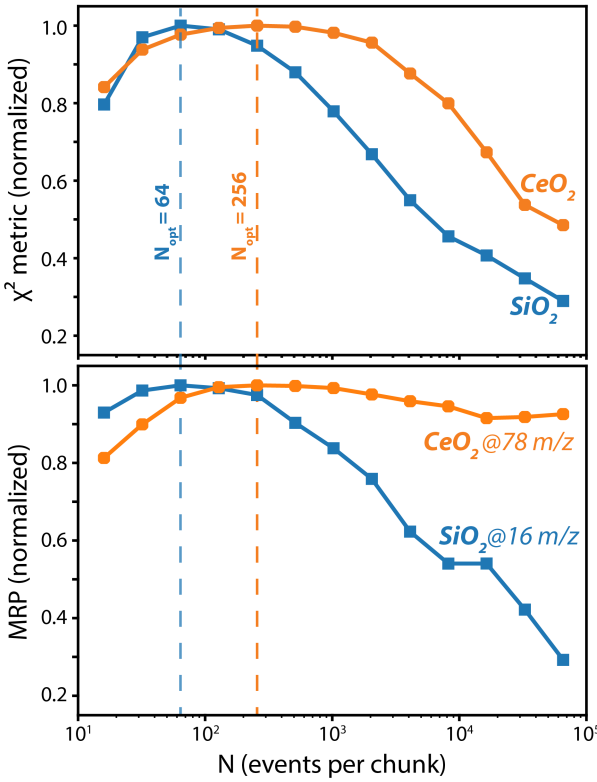

Figure 7: Determination of the chunk size parameter, N. Each dataset is divided into two subsets. The first subset is used to determine the correction factors which are then used to correct the second subset. (top) The χ^2 statistic – comparing the resulting mass spectrum to a uniform distribution – is computed and plotted for various choices of N. (bottom) The normalized mass-resolving power (MRP) (proportional to the reciprocal of the full width at half maximum of a peak, $\propto \frac{1}{\mathrm{FWHM}}$) of the most prominent peak in each dataset is plotted for comparison. An estimate of the optimal chunk size, N_{opt}, that is free from user selection bias occurs when the χ^2 and MRP is maximized. The CeO_2 and SiO_2 datasets have slightly different optimal chunk size parameters, but for both datasets the plots of χ^2 and MRP have a similar unimodal appearance.

The optimal chunk size will be related to the nature of the fluctuations in the accelerating voltage which can vary based on the sample and experimental conditions (Figure 7). For example, for the SiO_2 data the average gradient of the fluctuating acceleration voltage is relatively high, so a smaller chunk size is optimal. For the CeO_2 data the average gradient of the fluctuating acceleration voltage was lower, so a somewhat larger chunk size was optimal, with a significantly flatter peak in the χ^2 value as a function of chunk size. In any case, an estimate of the optimal chunk size can be objectively determined for each dataset.

6. Discussion

The algorithm developed here is predicated on the self-similarity of mass spectra collected at different points in time in an atom probe experiment. The time-of-flight histories in this manuscript were cropped to show only one or a few peaks for visualization. However, we emphasize that the full spectrum was used in the computation. We chose to use the full spectrum instead of simply a single peak in order to maximize the use of information. The better the information is used, the smaller the chunk size can be without risking overfitting, and the more thoroughly the voltage-drop effect can be corrected. A more straightforward algorithm that tracks only a single peak would fail to use information effectively. Regardless of the algorithm that is used to correct the data for a varying acceleration voltage, it is necessary that the user verify that the algorithm is yielding a reasonable result. For example, in this work, the SED corrected time-of-flight history was always inspected to visually verify the result.

The main assumption this algorithm makes is that each chunk of data can be corrected by a single multiplicative correction factor which can be empirically determined by comparison to a reference spectrum. If the reference spectrum is not representative of some portion of the dataset, for example if the tip position is changed or the material is heterogeneous, then the algorithm will not be effective. But so long as the physical geometry of the experiment is not altered then the SED correction should be practical. For example, changes in standing voltage, laser pulse energy, and laser pointing will be corrected by the SED algorithm. For relatively homogenous materials, the reference spectrum is most naturally chosen to be the spectrum of the full dataset and should be sufficient. The same method could even be applied towards determining bowl and voltage corrections, notably, without the need for selecting a single peak.

In contrast, for heterogeneous materials where the composition significantly changes throughout the dataset, the use of a single reference spectrum may be insufficient. In this case, a method would need to be devised to intelligently construct a set of reference spectra which could be independently compared to each chunk and scored. This extension of the SED correction algorithm would be able to leverage the numerous unsupervised machine learning techniques that are well-suited to this task. Future work will explore this possibility.

7. Conclusions

In conclusion, we observed that the standard voltage correction typically used for atom probe data analysis is insufficient when applied to data from strongly insulating samples. This failure was attributed to electrostatic effects and resulted in a poor-quality mass spectrum. We developed a computationally tractable algorithm to correct for the resulting systematic energy deficit that is based on the self-similarity of the mass spectra throughout a dataset. When this algorithm was applied to SiO_2 and CeO_2 datasets it significantly improved the quality of the mass spectra; decreasing the peak width and removing spurious (unphysical) peaks. This method should allow for more accurate peak identification and quantification of

the mass spectra of insulating samples on laser-triggered straight-flight-path atom probe instruments.

Acknowledgments

We gratefully acknowledge financial support from the NIST Innovations in Measurement Science (IMS) program.

References

[1] B. Gault, M. P. Moody, J. M. Cairney, S. P. Ringer, Atom Probe Microscopy, Vol. 160 of Springer Series in Materials Science, Springer New York, New York, NY, 2012. doi:10.1007/978-1-4614-3436-8.
URL http://link.springer.com/10.1007/978-1-4614-3436-8

[2] D. J. Larson, T. J. Prosa, R. M. Ulfig, B. P. Geiser, T. F. Kelly, Local Electrode Atom Probe Tomography, Springer New York, New York, NY, 2013. doi:10.1007/978-1-4614-8721-0.
URL http://link.springer.com/10.1007/978-1-4614-8721-0{_}5http://link.springer.com/10.1007/978-1-4614-8721-0

[3] M. K. Miller, R. G. Forbes, Atom-Probe Tomography, Springer US, Boston, MA, 2014. doi:10.1007/978-1-4899-7430-3.
URL http://link.springer.com/10.1007/978-1-4899-7430-3

[4] C. Pareige, W. Lefebvre-Ulrikson, F. Vurpillot, X. Sauvage, Atom Probe Tomography, Elsevier, Cambridge, MA, 2016.

[5] L. Arnoldi, M. Borz, I. Blum, V. Kleshch, A. Obraztsov, A. Vella, Effect of laser illumination on the electrical conductivity of single-crystal diamond needles, Journal of Applied Physics 126 (4) (2019) 045710. doi:10.1063/1.5092459.
URL http://aip.scitation.org/doi/10.1063/1.5092459

[6] Y. Chen, T. Ohkubo, K. Hono, Laser assisted field evaporation of oxides in atom probe analysis, Ultramicroscopy 111 (6) (2011) 562–566. doi:10.1016/j.ultramic.2010.12.013.
URL http://dx.doi.org/10.1016/j.ultramic.2010.12.013https://linkinghub.elsevier.com/retrieve/pii/S0304399110003554

[7] L. Arnoldi, E. P. Silaeva, A. Gaillard, F. Vurpillot, I. Blum, L. Rigutti, B. Deconihout, A. Vella, Energy deficit of pulsed-laser field-ionized and field-emitted ions from non-metallic nano-tips, Journal of Applied Physics 115 (20) (2014) 203705. doi:10.1063/1.4879315.
URL http://dx.doi.org/10.1063/1.4879315http://aip.scitation.org/doi/10.1063/1.4879315

[8] L. Arnoldi, E. Silaeva, F. Vurpillot, B. Deconihout, E. Cadel, I. Blum, A. Vella, Role of the resistivity of insulating field emitters on the energy of field-ionised and field-evaporated atoms, Ultramicroscopy 159 (2015) 139–146. doi:10.1016/j.ultramic.2014.11.018.
URL http://dx.doi.org/10.1016/j.ultramic.2014.11.018https://linkinghub.elsevier.com/retrieve/pii/S0304399114002332

[9] E. W. Müller, S. Krishnaswamy, Energy deficits in pulsed field evaporation and deficit compensated atom-probe designs, Review of Scientific Instruments 45 (9) (1974) 1053–1059. doi:10.1063/1.1686808.
URL http://aip.scitation.org/doi/10.1063/1.1686808

[10] A. Cerezo, T. J. Godfrey, S. J. Sijbrandij, G. D. W. Smith, P. J. Warren, Performance of an energy-compensated three-dimensional atom probe, Review of Scientific Instruments 69 (1) (1998) 49–58. doi:10.1063/1.1148477.
URL http://aip.scitation.org/doi/10.1063/1.1148477

[11] G. L. Kellogg, Field ion microscopy and pulsed laser atom-probe mass spectroscopy of insulating glasses, Journal of Applied Physics 53 (9) (1982) 6383–6386. doi:10.1063/1.331509.
URL http://aip.scitation.org/doi/10.1063/1.331509

[12] B. W. Caplins, SEDCORR: An Algorithm for Correcting Systematic Energy Deficits in the Atom Probe Mass Spectra (2019). doi:10.18434/M32166.

[13] M. Choueib, A. Ayari, P. Vincent, S. Perisanu, S. T. Purcell, Evidence for Poole–Frenkel conduction in individual SiC nanowires by field emission transport measurements, Journal of Applied Physics 109 (7) (2011) 073709. doi:10.1063/1.3556736.
URL http://aip.scitation.org/doi/10.1063/1.3556736

[14] J. W. Cooley, P. A. W. Lewis, P. D. Welch, The Fast Fourier Transform and Its Applications, IEEE Transactions on Education 12 (1) (1969) 27–34. doi:10.1109/TE.1969.4320436.
URL http://ieeexplore.ieee.org/document/4320436/

[15] T. Hastie, R. Tibshirani, J. Friedman, Model Assessment and Selection, in: The Elements of Statistical Learning, Springer, 2009, pp. 219–259. doi:10.1007/978-0-387-84858-7_7.
URL http://link.springer.com/10.1007/978-0-387-84858-7{_}7